Results in Physics 21 (2021) 103839

Contents lists available at ScienceDirect

Results in Physics

journal homepage: www.elsevier.com/locate/rinp

Prediction of mechanical and radiation parameters of glasses with high Bi_2O_3 concentration

A. El-Denglawey [a,b,*], Hesham M.H. Zakaly [c,d,*], K. Alshammari [e,f], Shams A.M. Issa [d,g], H. O. Tekin [h,i], Waheed S. AbuShanab [j], Yasser B. Saddeek [d,k]

[a] Department of Physics, College of University College at Turabah, Taif University, P.O. Box 11099, Taif 21944, Saudi Arabia
[b] Nano & Thin Film Lab., Department of Physics, Faculty of Science, South Valley University, Qena 83523, Egypt
[c] Institute of Physics and Technology, Ural Federal University, Ekaterinburg 620000, Russia
[d] Physics Department, Faculty of Science, Al-Azhar University, Assiut 71524, Egypt
[e] Department of Physics, Faculty of Arts and Sciences, Northern Border University, Saudi Arabia
[f] Faculty of Medical Sciences, Newcastle University, United Kingdom
[g] Physics Department, Faculty of Science, University of Tabuk, Tabuk 71451, Saudi Arabia
[h] Medical Diagnostic Imaging Department, College of Health Sciences, University of Sharjah, Sharjah 27272, United Arab Emirates
[i] Uskudar University, Medical Radiation Research Center (USMERA), 34672 Istanbul, Turkey
[j] Marine Engineering Department, Faculty of Maritime Studies and Marine Engineering, King Abdulaziz University, Jeddah 21589, Saudi Arabia
[k] Department of Physics, College of Science in Zulfi, Majmaah University, Al-Majmaah 11952 Saudi Arabia

ARTICLE INFO

Keywords:
Bismuthate based glasses
XCOM database
FLUKA code

ABSTRACT

This study aims to perform multidirectional characterizations on nuclear shielding efficiencies on some bismuth-based glasses. Accordingly, the γattenuation coefficients for xBi_2O_3-(75-x)B_2O_3–25Li_2O (x = 0, 10, 20, 30, 40, 50, 60 the 70 mol%) were widely evaluated using simulations and theoretical methods. Linear attenuation coefficient (LAC) of the glasses was obtained by the Monte Carlo general-purpose simulation code FLUKA and compared with the XCOM database up to 15 MeV. Moreover, LAC values have been utilized to evaluate related parameters like mass attenuation coefficient (MAC), total molecular cross-section (σ_t), total atomic cross-section (σ_a), half-value layer (HVL), total electronic cross-section (σ_e), mean free path (MFP), effective atomic number (Z_{eff}), and effective electron density (N_{eff}). The results noted that the XCOM and FLUKA data of the shielding parameters are in great agreement. Relatively higher density (5.818 g/cm^3), greater LAC, MAC, Zeff, and lower HVL, MFP values are achieved for 70Bi_2O_3-5B_2O_3–25Li_2O glass. Accordingly, this glass sample is a better gamma shield.

Introduction

The promising nuclear technologies based on ionizing radiation are part of our daily life from medical applications to food sanitization in today's World. On the other hand, such widespread use of radiation does not mean ignoring its harmful effects. On the contrary, a potential situation of widespread use of ionizing radiation is the obvious increase in the amount of radiation emitted from artificial sources to the society and the environment. The ALARA has determined the most applicable protection methods to date (**As Low As Reasonably Achievable**) principle. The ALARA principle emphasizes that while maximizing the possible exposure time at the farthest distance from the radiation source, it is also necessary to consider the maximum shielding procedures. At the beginning of the development of radiation technology, there were its professional victims-physicists, radiologists, radio chemists-researchers who studied the properties and applications of these energy radiations, without evaluating their ability to have a destructive effect on living matter. However, the society soon realized the harm that energy radiation could cause when exposed to uncontrolled radiation, and since then it has worked diligently to understand the biological effects of radiation further and establish acceptable dose limits [1,2]. Besides, the development of nuclear reactors and the generation of large amounts of nuclear waste had created a significant concern for public health.

Accordingly, governments have figured out that rapid actions are needed to guard radiation operators and the community from radiation in term of its potential risks on vital biological structures. As every

* Corresponding authors.
E-mail addresses: a.denglawey@tu.edu.sa (A. El-Denglawey), h.m.zakaly@azhar.edu.eg (H.M.H. Zakaly).

https://doi.org/10.1016/j.rinp.2021.103839
Received 12 November 2020; Received in revised form 1 January 2021; Accepted 10 January 2021
Available online 14 January 2021

Table 1
Chemical composition (mol%) and elements (wt. %) and density for glasses.

Code	Bi_2O_3	B_2O_3	Li_2O	Li	B	O	Bi	ρ (g/cm^3)
LBBi0	0	75	25	0.0581	0.2717	0.6702	0.0000	2.377
LBBi10	10	65	25	0.0349	0.1415	0.4027	0.4208	3.487
LBBi20	20	55	25	0.0250	0.0856	0.2879	0.6016	4.242
LBBi30	30	45	25	0.0194	0.0545	0.2240	0.7021	4.901
LBBi40	40	35	25	0.0159	0.0347	0.1833	0.7661	5.342
LBBi50	50	25	25	0.0135	0.0210	0.1551	0.8105	5.598
LBBi60	60	15	25	0.0117	0.0109	0.1345	0.8430	5.759
LBBi70	70	5	25	0.0103	0.0032	0.1186	0.8679	5.818

radionuclide consumer knows, the result has been adopting comprehensive legislation, the establishment of regulatory bodies and licensing mechanisms, the establishment of radiation exposure standards, and the requirement to train radiation workers following accepted practices for dealing with radiation and radionuclides [3,4]. The shielding procedures have been hitherto provided with traditional materials such as concrete and Lead (Pb). However, as with any innovation brought by technology, there are some notable innovations in this case. IAEA (International Atomic Energy Agency) and WHO (World Health Organization) encouraged researchers to develop new generation shielding materials to replace traditional shielding materials due to their deficiency in physical and structural properties. Among the investigated new generation shielding materials, glass materials attracted relatively more attention from the scientific community. The glasses have their unique advantages as a useful material for radiation shielding. The concrete remarked by several drawbacks associated with its usage as radiation shielding material. The unsafe nature of Lead and the cracks could be easily created through it after a prolonged exposure to environmental influences. The most important advantages that the glassy material can be a good substitute of concrete and Lead are the transparency, the good homogeneity and the ease of fabrication. The glassy material's mass attenuation coefficient can be increased by inserting the heavy elements in the glass matrix. Glass materials are promising shielding barriers because they have a highly suitable range for hosting different types of heavy metal elements in their matrix [5–7]. Therefore, in the late time, various glass materials have been utilized for nuclear applications because they perform both tasks by allowing visibility while exposure to radiations and working as an efficient protection barrier. An effective glass shield should provide a high interaction cross-section value. Besides, its rigidity and optical parameters should be affected by irradiation as a minimum. Many studies have been focused on investigating gamma-ray attenuation in various types of glass shielding have been achieved [8–10]. Li_2O-B_2O_3 glasses are traditional glass systems created over a wide range [11–13]. Due to the essential feature of those glasses in-field storage batteries, they have been extensively studied. Moreover, due to the higher valance of oxides like Bi_2O_3, it is used as a modifier to make significant structural effects. Thus, these glass materials' physical parameters display jump changes with such switching of the function of the cations [14,15]. The Bi_2O_3-glass materials greatly affect their applications in various fields such as glass, ceramics, sensors, and reflecting windows [16–18].

J. Kaewkhao et al. [19] investigated the mass attenuation coefficients and shielding parameters of borate based glasses involving Bi_2O_3 and BaO. They [19] establish that the increment of the mass attenuation coefficients is function of Bi_2O_3, BaO and PbO contents. Furthermore, the half-value layers of investigated glasses are favourable than normal concretes and marketable window glasses. These results reflect that the Bi-based glass can replace Pb in radiation shielding glass [19]. P. Limkitjaroenporn et al. prepared the lead sodium borate glasses via melt-quenching and explored their optical, physical, structural and gamma-rays shielding properties. They recorded that gamma-ray shielding properties increased with increase in PbO concentration [20]. K.Kirdsiri et al. measured the radiation shielding and optical properties of bismuth lead silicate and barium silicate glasses. They observed that total mass attenuation coefficients of the glasses at energy 662 keV are enhanced by the increment of Bi_2O_3 and PbO, which elevated the photoelectric absorption in the glass networks [21]. S. Kaewjang et al. fabricated and investigated the (80–x)B_2O_3-10SiO_2-10CaO-xGd_2O_3 (where x = 15, 20, 25, 30 and 35 mol%) for their radiation shielding, physical and optical properties. They found that the experimental values of mass attenuation coefficients, effective atomic number and effective electron densities of the glasses increase with the increasing of Gd_2O_3 concentration and also with the decreasing of photon energy from 223 to 662 keV [22]. N.Chanthima et al. investigated the impacts of BaO on the physical properties of zinc borate based glasses. They recorded that the radiation shielding paramters are enhanced as a function of BaO, and the decrement of γ-ray energy [23]. K.Boonin et al. synthesized and inspected the zinc barium tellurite glasses for their defensive radiation mechanism and structural behavior. The results found that the effective atomic number and effective electron density decrease with the increase in γ-ray energies which is in a good agreement with theoretical values attained using Geant4 and WinXCOM [24]. W.Cheewasukhanont et al. studied the radiation shielding parameres of bismuth borosilicate based glasses. The outcomes revealed that the density of the glasses increase with the increase of Bi2O3 content, while its particle size does not incorporate for the density. They found that the radiation shielding parameters of these glasses are enhanced than that for traditional glass-window and for some types of concrete [25]. S.Kaewjaeng et al. prepared and investigated (80-x) B_2O_3:10SiO_2:10 CaO:xLa_2O_3 glass (where × = 10, 15, 20, 25 and 30 mol %) for x-ray shielding, physical and optical properties. The found that the half-value layer and ten-value layer of glass samples tend to decrease when the kVp of an x-ray instrument decrease and La_2O_3 concentrations increase [26]. F. H. ElBatal et al. they studied UV–visible, FTIR absorption spectra of some prepared undoped and NdF3-doped borophosphate glasses with varying dopant contents before and after gamma irradiation [27]. H. ElBatal et al. prepared undoped and CuO-doped lithium phosphate, lead phosphate and zinc phosphate glasses. The measured the UV–visible and infrared absorption spectra of the prepared samples before and after successive gamma irradiation [28]. H. M. Diab et al. deliberate the dosimetric impact of low absorbed dose in a modified borate bioactive glass as utilization for such newly studied material. The outcoming showed that the ideal grain size is extended between 53 and 106 μm respecting to glow peak of borate bioactive glass after gamma irradiation from gamma radiation cobalt source, three unresolved glow peaks was founded [29]. Therefore, this work aims to improve the effectiveness of gamma radiation protection of glasses derived from heavy metals xBi_2O_3-(75-x)B_2O_3–25Li_2O.

Materials and methods

A traditional melt-quench tool is utilized to fabricate glass samples of the Bi_2O_3-B_2O_3–Li_2O system. The samples were coded as tabulated in Table 1. Desired amounts from Bi_2O_3, Li_2CO_3, and H_3BO_3 (Analar grade) are blended and fused in an open ceramic melting-pot crucible at about 1350 K for 1.5 h. The melting-pot was rotated several times during the melting process. The melt was poured into a preheated brass mold, and the result glass samples were annealed at about 550 K for 1 h. After

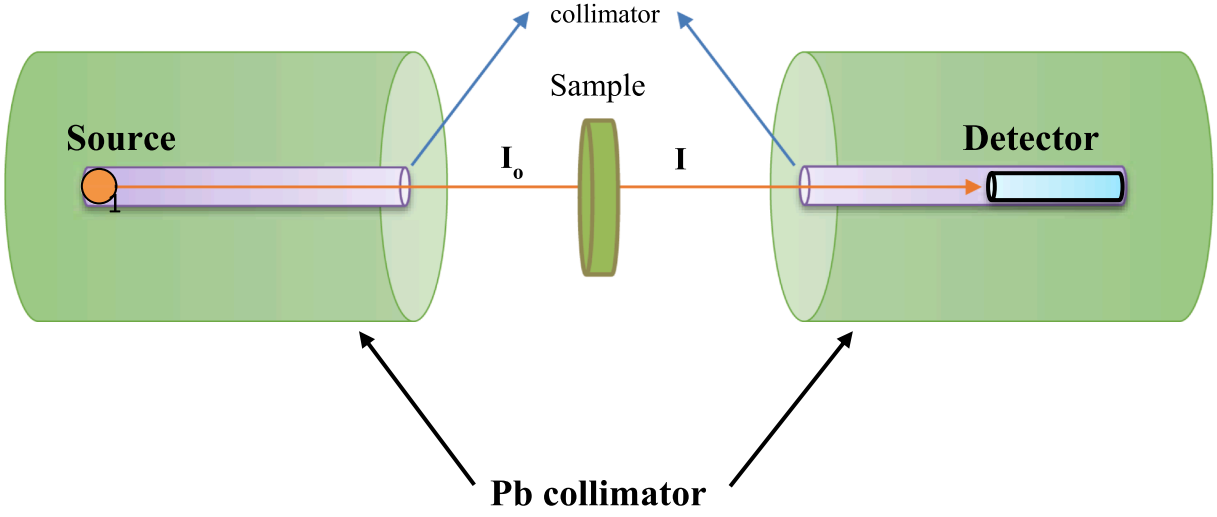

Fig. 1. FLUKA Monte Carlo simulation setup used for mass attenuation coefficients calculations of glasses.

annealing, the values of the density (ρ) of the samples were acquired via the Archimedes method (Toluene is the buoyant liquid).

The γ-ray shielding properties were computed using FLUKA and XCom for gamma photons ranged from 0.015 MeV to 15 MeV. If an absorber is placed between the radioactive source and the detector, the emitted photons decrease exponentially through the glass due to the Beer-Lambert law [30,31]:

$$I = I_o e^{-\mu x} \tag{1}$$

I_o is the intensity of initially γbeam and I the intensity of weaken γbeam through the glass. μis the linear attenuation coefficient, and quantity of × is the thickness of the glass. For the mixture of elements, the mass attenuation coefficients (MAC) will be computed using:

$$MAC = \sum_i w_i (MAC)_i \tag{2}$$

To calculate the effective atomic number (Z_{eff}) and effective electron density (N_{eff}) of prepared glasses, the total molecular cross-section (σ_t), total atomic cross-section (σ_a) and total electronic cross-section (σ_e) values should be obtained [32–34]:

$$\sigma_t = \frac{1}{N_A} \sum_i n_i A_i (MAC)_i \tag{3}$$

$$\sigma_a = \frac{1}{N_A} \sum_i f_i A_i (MAC)_i \tag{4}$$

$$\sigma_e = \frac{1}{N_A} \sum_i \frac{f_i A_i}{Z_i} (MAC)_i \tag{5}$$

$$Z_{eff} = \frac{\sigma_a}{\sigma_e} \tag{6}$$

$$N_{eff} = \frac{(MAC)}{\sigma_e} \tag{7}$$

where n_i, A_i, Z_i, f_i and N_A are the number of atoms, the atomic weight, the atomic number, fractional abundance of i^{th} element in a molecule and Avogadro number, respectively. The glass thickness, which reduces the initial photon intensity to 1/2, is termed half-value layer (HVL), and are obtained using the following equation [35–37]:

$$HVL = \frac{\ln(2)}{LAC} \tag{8}$$

The glass with 1 mean free path (MFP) thickness takes in 0.368 of the premier γintensity when it crosses through the sample [38,39]:

$$MFP = \frac{1}{LAC} \tag{9}$$

Another essential parameter in radiation shielding is the radiation protection efficiency (RPE) [26]:

$$RPE(\%) = \left(1 - \frac{I}{I_o}\right) \times 100 \tag{10}$$

FLUKA is the radiation transport code for Monte Carlo [40–42]. During the present simulation a MATERIAL card attached in addition to the COMPOUND cards required to identify the samples. The MATERIAL card showed the chosen composition, name, density, material number, etc. of the compound. NaI scintillation detector with a cylindrical shape (3 in. × 3 in.) was placed in a Pb-cylindrical collimator having a 12 cm outer and 0.2 cm inner diameter and 15 cm length. The NaI area was described by a USRTRACK scorecard as the track length fluctuation According to the statistical error (<0.1%), the simulations ranged from 10 to 20 million primary photons in total. A USRBIN card was used to measure the scattering of a photon within the volume of the detector. A BEAM card then defined the form and energy of the particle. In this analysis, a BEAM card was produced to set a monoenergetic photon (0.2 cm size) at energy values of 0.081, 0.356, 0.662, 1.173 and 1.33 MeV to determine the beam source. In addition, a BEAMPOS card was produces to adjust the direction and position of this beam source in the plus z-axis. The photon transmission power cut was adjusted to an energy level of 10^{-7} GeV with an EMFCUT card at low energy levels. To modeling of all glass samples, a cylindrical geometry with a diameter of 1.0 cm and thicknesses varying between 0.1 and 0.5 cm (according to the primary photon energy) were used. The glass specimens are formalized with a RPP body. It is denoted by 6 numbers called Xmin-Xmax, Ymin-Ymax and Zmin- Zmax and its boundaries are parallel to the coordinate axis. In this geometry, Xmax (Ymax) and Xmin (Ymin) have been chosen as +5 cm and −5cm, respectively [43]. As a result, a target material of 15 cm in long and width with various thicknesses specified by Zmax and Zmin was obtained. After the photons interacted with the sample, they were located in the detector volume. The detector volume is covered with Pb collimator to block determination of dispersed photons. On the other hand, The FLUKA program, which is a simulation program, has been used to predict the MAC by acquiring both the photons passing through the material and the initial photon number in the detector volume [44]. In addition, USRBIN has been utilized as a detector card that enables to forecast the photon flux within a detector (Fig. 1).

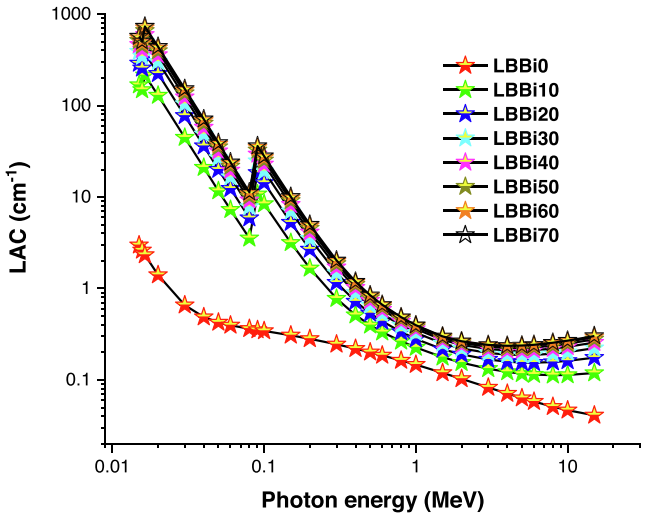

Fig. 2. Variation of linear attenuation coefficient (LAC) with photon energy for all glasses.

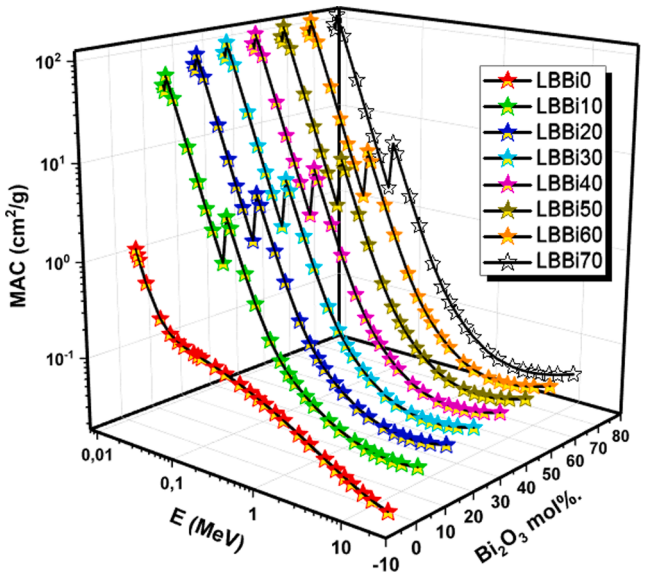

Fig. 3. Variation of mass attenuation coefficient (MAC) values for the glass samples with photon energy.

Results and discussion

The optical parameters of glass had high concentrations of Bi_2O_3 were discussed before [17,45]. The studies found that the higher amounts of Bi_2O_3 increase these glasses' density due to the ideal molecular weight of Bi_2O_3. The higher contents of Bi_2O_3 expand the glass network by increasing both the bond length of BO_3 structural units and the oxygen environment around Bi_2O_3. As reflected from the structural analysis of these glasses, this process decreases the optical band gap and increases the refractive indices of the investigated glasses. Moreover, the addition of B_2O_3 to this type of glasses transform the characteristic yellow shift of Bi_2O_3 to redshift positions [17,46] so boro-bismuthate glasses will be a good candidate for transparent radiation shieldings.

The composition and density (ρ) of glasses are shown in Table 1. As presented in this table, the ρvalues rise from 2.377 to 5.818 (g/cm^3) with increment **Bi_2O_3** content from 0 to 70 wt%. Fig. 2 shows the variation of LAC in LBBi0, LBBi10, LBBi20, LBBi30, LBBi40, LBBi50, LBBi50 and LBBi70 glass samples with photon energy ranged from 0.015to15 MeV. In the mentioned figure, the LAC values rise with increment Bi_2O_3 concentration.

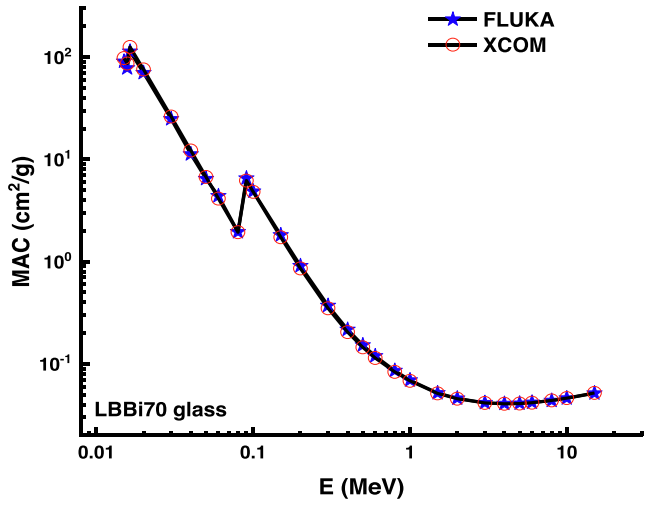

Fig. 4. Comparison of XCOM and FLUKA codes computed mass attenuation coefficients (MAC) versus photon energy for LBBi70 glass sample.

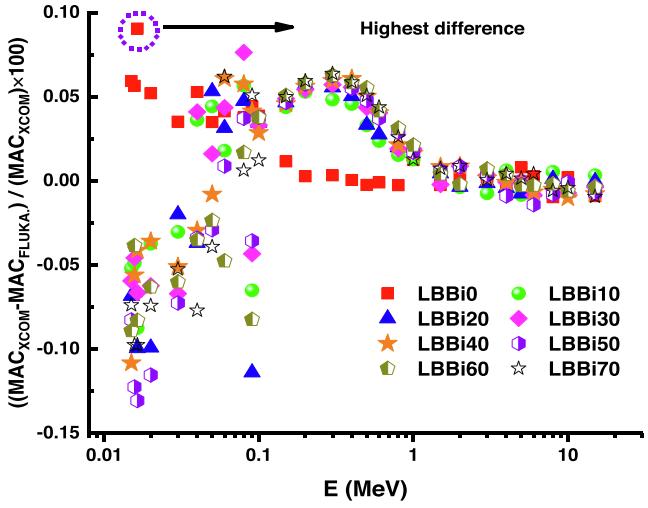

Fig. 5. Relative differences (RD) between XCOM and FLUKA code for all glasses.

The FLUKA code and XCOM database results for the investigated glasses are shown in Fig. 3. A considerable agreement between FLUKA code and XCOM database values is presented. In Fig. 3, MAC values depend on both energy and Bi_2O_3 content. The MAC values for all glasses reduce with increment energy from 0.015 to 15 MeV. Moreover, it must be noted that this behavior may be attributed to the domination of the photoelectric effect (PE), Compton scattering (CS) and pair production (PP) at low, medium and high energy ranges, respectively. As an example, Fig. 4 present the MAC values obtained via XCOM and FLUKA codes against energy for LBBi70 sample, which have excellent agreement between simulation and theoretical calculations. Furthermore, little differences between FLUKA and XCOM values. It is indicated that there is a small variance in MAC values due to the accuracy of the FLUKA geometry design. To get extra prudence into the validity of the calculations, relative differences (RD, %) between the results with XCOM database and FLUKA code were estimated. Fig. 5 describes the RD of theoretical between simulated concerning values for gamma energies of 0.015 to 15 MeV. The $RD_{XCOM.-\ FLUKA}$ and was calculated by:

$$RD_{XCOM-FLUKA}(\%) = \frac{(MAC)_{XCOM} - (MAC)_{FLUKA}}{(MAC)_{XCOM}} \times 100 \quad (11)$$

Table 2
mass attenuation coefficient (cm^2/g) results for all glass samples.

E (MeV)	LBBi0			LBBi10			LBBi20			LBBi30		
	FLUKA	XCOM	Δ	FLUKA	XCOM	Δ	FLUKA	XCOM	Δ	FLUKA	XCOM	Δ
0.015	1.3261	1.25	6%	45.61	48.12	−5%	63.58	68.26	−7%	74.73	79.45	−6%
0.02	0.6226	0.59	5%	35.63	37.02	−4%	47.44	52.66	−10%	57.53	61.36	−6%
0.03	0.2861	0.28	4%	12.44	12.83	−3%	17.87	18.23	−2%	19.80	21.23	−7%
0.04	0.2158	0.21	5%	6.23	6.02	4%	8.20	8.51	−4%	10.31	9.90	4%
0.05	0.1857	0.18	3%	3.50	3.35	4%	4.96	4.71	5%	5.55	5.47	2%
0.06	0.1736	0.17	4%	2.13	2.09	2%	3.00	2.91	3%	3.52	3.37	4%
0.08	0.1588	0.15	4%	1.07	1.02	6%	1.45	1.39	5%	1.72	1.60	8%
0.10	0.1501	0.14	4%	2.49	2.41	4%	3.49	3.38	3%	4.05	3.92	3%
0.15	0.1310	0.13	1%	0.95	0.91	4%	1.30	1.24	5%	1.49	1.43	5%
0.20	0.1190	0.12	0%	0.50	0.48	5%	0.67	0.63	6%	0.75	0.72	5%
0.30	0.1036	0.10	0%	0.23	0.22	5%	0.29	0.27	6%	0.32	0.30	6%
0.40	0.0926	0.09	0%	0.15	0.15	5%	0.18	0.17	5%	0.19	0.18	6%
0.50	0.0844	0.08	0%	0.12	0.11	3%	0.13	0.13	3%	0.14	0.13	4%
0.60	0.0782	0.08	0%	0.10	0.10	2%	0.11	0.10	3%	0.11	0.11	4%
0.80	0.0686	0.07	0%	0.08	0.08	2%	0.08	0.08	2%	0.08	0.08	2%
1.00	0.0626	0.06	1%	0.07	0.06	1%	0.07	0.07	2%	0.07	0.07	2%
1.50	0.0502	0.05	0%	0.05	0.05	1%	0.05	0.05	0%	0.05	0.05	0%
2.00	0.0434	0.04	0%	0.04	0.04	0%	0.04	0.04	0%	0.05	0.05	1%
3.00	0.0349	0.03	0%	0.04	0.04	−1%	0.04	0.04	0%	0.04	0.04	0%
4.00	0.0297	0.03	0%	0.04	0.04	1%	0.04	0.04	0%	0.04	0.04	0%
5.00	0.0269	0.03	1%	0.03	0.03	−1%	0.04	0.04	−1%	0.04	0.04	0%
6.00	0.0245	0.02	0%	0.03	0.03	0%	0.04	0.04	−1%	0.04	0.04	−1%
8.00	0.0212	0.02	−1%	0.03	0.03	1%	0.04	0.04	0%	0.04	0.04	0%
10.00	0.0197	0.02	0%	0.03	0.03	−1%	0.04	0.04	−1%	0.04	0.04	−1%
15.00	0.0171	0.02	−1%	0.03	0.03	0%	0.04	0.04	0%	0.05	0.05	0%
E (MeV)	LBBi40			LBBi50			LBBi60			LBBi70		
	FLUKA	XCOM	Δ	FLUKA	XCOM	Δ	FLUKA	XCOM	Δ	FLUKA	XCOM	Δ
0.015	77.20	86.58	−11%	83.95	91.52	−8%	86.66	95.14	−9%	90.67	97.91	−7%
0.02	64.49	66.90	−4%	62.57	70.74	−12%	68.91	73.55	−6%	70.08	75.70	−7%
0.03	21.96	23.14	−5%	22.68	24.46	−7%	23.90	25.43	−6%	24.79	26.17	−5%
0.04	10.46	10.78	−3%	11.01	11.40	−3%	11.43	11.85	−4%	11.25	12.19	−8%
0.05	5.90	5.95	−1%	6.10	6.28	−3%	6.37	6.53	−2%	6.45	6.71	−4%
0.06	3.89	3.66	6%	3.90	3.87	1%	3.82	4.02	−5%	4.38	4.13	6%
0.08	1.83	1.73	6%	1.89	1.82	4%	1.92	1.88	2%	1.95	1.94	1%
0.10	4.38	4.26	3%	4.67	4.50	4%	4.85	4.68	4%	4.87	4.81	1%
0.15	1.61	1.54	5%	1.70	1.63	5%	1.77	1.69	5%	1.82	1.73	5%
0.20	0.81	0.77	6%	0.85	0.81	6%	0.88	0.84	6%	0.91	0.86	6%
0.30	0.34	0.32	6%	0.35	0.33	6%	0.36	0.34	6%	0.37	0.35	6%
0.40	0.20	0.19	6%	0.21	0.20	5%	0.21	0.20	6%	0.22	0.20	6%
0.50	0.14	0.14	5%	0.15	0.14	5%	0.15	0.14	6%	0.15	0.14	5%
0.60	0.11	0.11	4%	0.12	0.11	4%	0.12	0.11	4%	0.12	0.11	4%
0.80	0.08	0.08	2%	0.08	0.08	3%	0.09	0.08	3%	0.09	0.08	3%
1.00	0.07	0.07	2%	0.07	0.07	2%	0.07	0.07	2%	0.07	0.07	1%
1.50	0.05	0.05	1%	0.05	0.05	1%	0.05	0.05	0%	0.05	0.05	1%
2.00	0.05	0.05	1%	0.05	0.05	1%	0.05	0.05	0%	0.05	0.05	1%
3.00	0.04	0.04	0%	0.04	0.04	0%	0.04	0.04	1%	0.04	0.04	0%
4.00	0.04	0.04	0%	0.04	0.04	−1%	0.04	0.04	0%	0.04	0.04	0%
5.00	0.04	0.04	0%	0.04	0.04	0%	0.04	0.04	0%	0.04	0.04	0%
6.00	0.04	0.04	−1%	0.04	0.04	−1%	0.04	0.04	0%	0.04	0.04	0%
8.00	0.04	0.04	−1%	0.04	0.04	−1%	0.04	0.04	0%	0.04	0.04	−1%
10.00	0.04	0.04	−1%	0.04	0.04	0%	0.05	0.05	−1%	0.05	0.05	0%
15.00	0.05	0.05	−1%	0.05	0.05	−1%	0.05	0.05	0%	0.05	0.05	−1%

Table 2 presents the MAC values for all glasses increment as the Bi_2O_3 content rise from 0 to 70 mol—% at studied energy. LBBi70 glass has the highest MAC values among investigated samples, which is a super γ-ray absorber.

HVL and MFP are the necessary parameters to estimate a material's gamma shielding capacity, and ordinarily, the smaller these values, the higher the shielding performance. Fig. 6, and Fig. 7 showing that the MFP and HVL values variation for LBBi0, LBBi10, LBBi20, LBBi30, LBBi40, LBBi50, LBBi50 and LBBi70 samples against energy. As the energy rise, the HVL, and MFP increment rapidly. Due to the HVL and MFP values depending upon the energy corresponding to PE, CS and PP interactions dominate at low, medium and high energy. Moreover, the HVL, and MFP values, reduce with increment Bi_2O_3 content for LBBi0, LBBi10, LBBi20, LBBi30, LBBi40, LBBi50, LBBi50 and LBBi70 samples. LBBi70 sample has the lowest HVL, and MFP values compared to the remaining glasses. Fig. 8 represents the HVL) values versus energy for LBBi70 sample, concretes (OC, HSC, ILC, IL and SSC) [47] and glasses (G1 and G2) [48]. As compared in energy range, LBBi70 sample has the lowest HVL value comparing to concretes and glasses. Fig. 9 shows the tenth-value layer (TVL) change with energy for all glasses, which ensure that as LBBi70 contains lower TVL and therefore have a higher MAC than the other samples.

The calculated (σ_t, σ_a, and σ_e) values for glasses have been presented in Table 3, respectively. All these values present almost the same behavior that for MAC against energy and Bi_2O_3 content. Z_{eff} and N_{eff} values for all samples are listed in Table 3. As shown in Fig. 10 and Table 3, the Z_{eff} and N_{eff} values depend on both energy and Bi_2O_3 content. Z_{eff} and N_{eff} values rise with an increment of Bi_2O_3 ratio and reduce as the energy increases. The sample trend of Z_{eff} and N_{eff} values is confirmed in Fig. 11. Among the studied glasses, LBBi70 has the Z_{eff} and

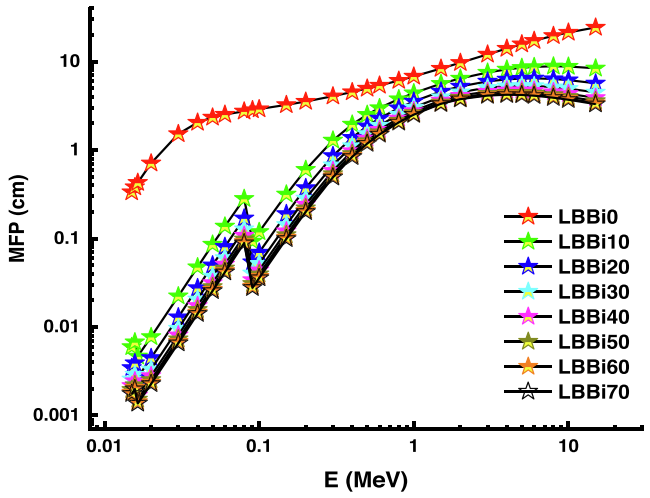

Fig. 6. Variations of mean free path (MFP) with photon energy for all glasses.

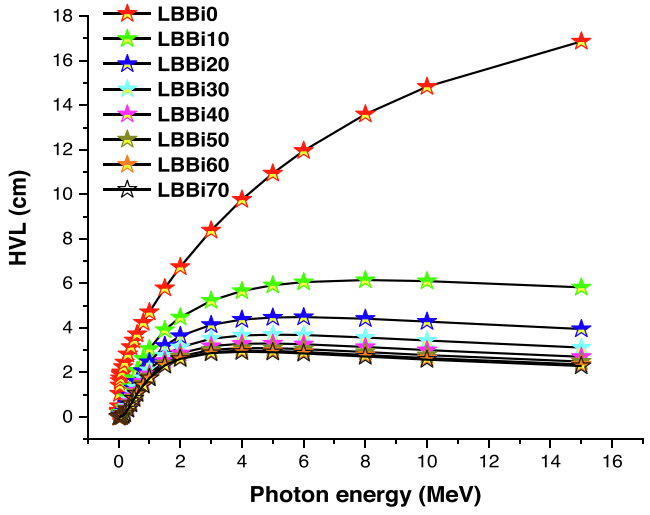

Fig. 7. Variations of half-value layer (HVL) with photon energy for all glasses.

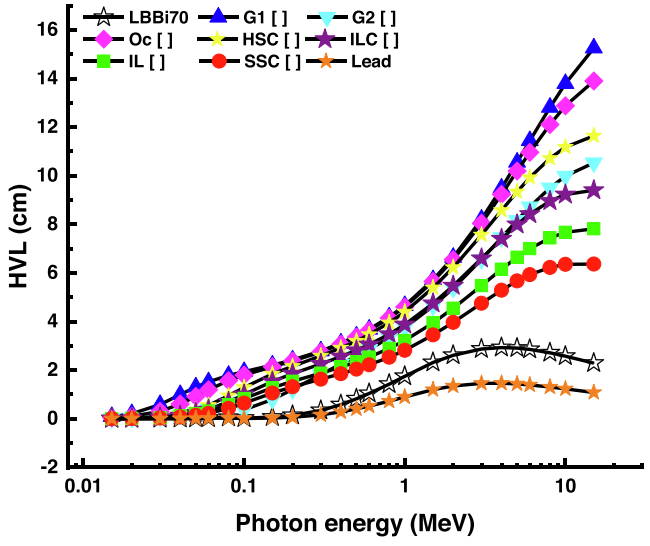

Fig. 8. Comparison of HVL of the LBBi70 glass with some commercial glasses.

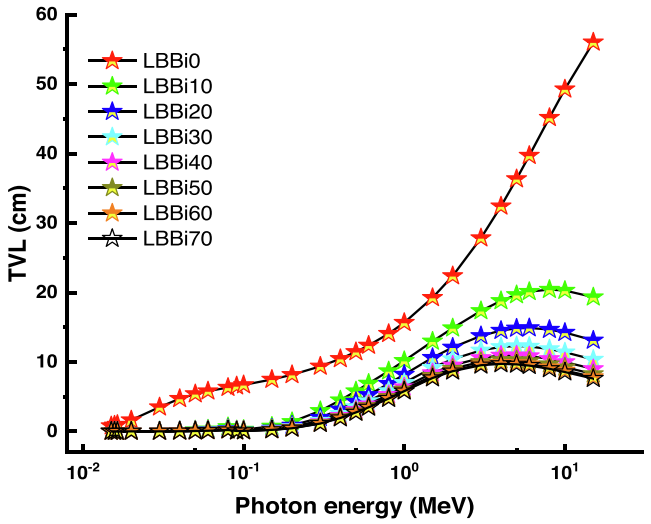

Fig. 9. Variations of half-value layer (TVL) with photon energy for all glasses.

Neff values at photon energy ranged from 0.15 to 15 MeV.

Bismuthate based glasses can be formed in a wide range with mixing Bi_2O_3 with small additions of B_2O_3 or alkalis such as Li_2O. In this case, a glass network from [BiO_3] and distorted [BiO_6] polyhedra will be built by establishing both network-forming and network modifying positions [17,46,49]. At small contents of Li_2O, Li^+ ions occupy the interstices of bismuthate network to match the excess negative charge of BiO_6 octahedra[50,51]. Due to these aspects, these glasses had numerous potential applications as fast ion conducting glasses [52] in optical-based devices [53] and thermal sensors[54]. On the other hand, the elastic properties of glasses can significantly notify their structure because its rigidity can present the structure. The elastic properties are investigated via determining the ultrasonic velocities and the glasses' density [55]. Moreover, the elastic properties of glasses can be defined according to the bond compression model [56,57]. This model computes the bulk modulus (KBC) and Young's modulus (YBC) from the molar chemical formula of the glass and some other physical parameters considering the ratio N4 [58] which is the ratio of four-to three-coordinate boron in the borate network as:

$$K_{BC} = \frac{N_A \sum_i X_i n_i r_i^2 F_i}{9V_m} \tag{12}$$

$$F = \frac{\sum_i X_i n_i f_i}{\sum_j X_j f_j} \tag{13}$$

$$f = 5.28\left(\frac{X_a X_b}{r^2}\right)^{3/4} + 30 \tag{14}$$

$$Y_{BC} = 3K_{BC}\left[1 - \frac{0.56}{L^{0.25}}\right] \tag{15}$$

$$L = \frac{\sum_i X_i n_i N_{ci}}{\sum_j X_j N_{ci}} \tag{16}$$

The nominations and the values of the preceding parameters were listed in Table 4. The increment of Bi_2O_3 content up to high concentrations in lithium borate network implies the existence of two glass network formers with high field strength cations. Bi_2O_3 has significant high density than that of Li_2O or B_2O_3 and moderate bond strength of Bi – O compared with B – O [59]. Also, Bi_2O_3 due to its high polarizability, it can modify its environment by creating bridging oxygens and increases the coordination number and the number of networks per unit volume of the glass network. So, the increment of Bi_2O_3 will increase the density of the lithium borate glasses and compact the glass network.

Table 3
Total molecular cross-sections (barn/atom) (σ_t), Total atomic cross-sections (barn/atom) (σ_a), Effective atomic number (Z_{eff}) and Effective electron density (N_{eff}) of all glasses.

	LBBi0	LBBi10	LBBi20	LBBi30	LBBi40	LBBi50	LBBi60	LBBi70
E (keV)	Total molecular cross-sections (barn/atom) (σ_t)							
0.015	1.18E−21	4.52E−20	6.41E−20	7.46E−20	8.13E−20	8.59E−20	8.93E−20	9.19E−20
0.02	5.56E−22	3.48E−20	4.94E−20	5.76E−20	6.28E−20	6.64E−20	6.91E−20	7.11E−20
0.03	2.60E−22	1.21E−20	1.71E−20	1.99E−20	2.17E−20	2.30E−20	2.39E−20	2.46E−20
0.04	1.93E−22	5.65E−21	7.99E−21	9.30E−21	1.01E−20	1.07E−20	1.11E−20	1.14E−20
0.05	1.68E−22	3.14E−21	4.42E−21	5.13E−21	5.59E−21	5.90E−21	6.13E−21	6.30E−21
0.06	1.57E−22	1.96E−21	2.74E−21	3.17E−21	3.44E−21	3.63E−21	3.77E−21	3.88E−21
0.08	1.44E−22	9.55E−22	1.30E−21	1.50E−21	1.62E−21	1.71E−21	1.77E−21	1.82E−21
0.10	1.36E−22	2.26E−21	3.17E−21	3.68E−21	4.00E−21	4.23E−21	4.39E−21	4.52E−21
0.15	1.22E−22	8.51E−22	1.16E−21	1.34E−21	1.45E−21	1.53E−21	1.58E−21	1.63E−21
0.20	1.11E−22	4.48E−22	5.92E−22	6.72E−22	7.23E−22	7.59E−22	7.85E−22	8.05E−22
0.30	9.70E−23	2.09E−22	2.57E−22	2.83E−22	3.00E−22	3.12E−22	3.21E−22	3.27E−22
0.40	8.69E−23	1.38E−22	1.60E−22	1.72E−22	1.80E−22	1.85E−22	1.89E−22	1.92E−22
0.50	7.94E−23	1.07E−22	1.19E−22	1.25E−22	1.29E−22	1.32E−22	1.34E−22	1.36E−22
0.60	7.35E−23	8.98E−23	9.68E−23	1.01E−22	1.03E−22	1.05E−22	1.06E−22	1.07E−22
0.80	6.46E−23	7.13E−23	7.42E−23	7.58E−23	7.68E−23	7.75E−23	7.80E−23	7.84E−23
1.00	5.81E−23	6.10E−23	6.22E−23	6.29E−23	6.34E−23	6.37E−23	6.39E−23	6.41E−23
1.50	4.73E−23	4.78E−23	4.80E−23	4.81E−23	4.82E−23	4.82E−23	4.83E−23	4.83E−23
2.00	4.06E−23	4.17E−23	4.21E−23	4.24E−23	4.25E−23	4.26E−23	4.27E−23	4.28E−23
3.00	3.27E−23	3.57E−23	3.70E−23	3.78E−23	3.82E−23	3.86E−23	3.88E−23	3.90E−23
4.00	2.80E−23	3.30E−23	3.51E−23	3.63E−23	3.70E−23	3.75E−23	3.79E−23	3.82E−23
5.00	2.50E−23	3.15E−23	3.43E−23	3.59E−23	3.69E−23	3.76E−23	3.81E−23	3.85E−23
6.00	2.29E−23	3.08E−23	3.42E−23	3.61E−23	3.73E−23	3.81E−23	3.87E−23	3.92E−23
8.00	2.01E−23	3.04E−23	3.47E−23	3.72E−23	3.87E−23	3.98E−23	4.06E−23	4.12E−23
10.00	1.85E−23	3.06E−23	3.58E−23	3.87E−23	4.05E−23	4.18E−23	4.27E−23	4.35E−23
15.00	1.62E−23	3.21E−23	3.88E−23	4.26E−23	4.50E−23	4.67E−23	4.79E−23	4.88E−23
E (keV)	LBBi0	LBBi10	LBBi20	LBBi30	LBBi40	LBBi50	LBBi60	LBBi70
	Total atomic cross-sections (barn/atom) (σ_a)							
0.015	9.04E−23	3.48E−21	4.93E−21	5.74E−21	6.25E−21	6.61E−21	6.87E−21	7.07E−21
0.02	4.28E−23	2.67E−21	3.80E−21	4.43E−21	4.83E−21	5.11E−21	5.31E−21	5.47E−21
0.03	2.00E−23	9.27E−22	1.32E−21	1.53E−21	1.67E−21	1.77E−21	1.84E−21	1.89E−21
0.04	1.48E−23	4.34E−22	6.15E−22	7.15E−22	7.79E−22	8.23E−22	8.55E−22	8.80E−22
0.05	1.30E−23	2.42E−22	3.40E−22	3.95E−22	4.30E−22	4.54E−22	4.71E−22	4.85E−22
0.06	1.20E−23	1.51E−22	2.10E−22	2.44E−22	2.65E−22	2.79E−22	2.90E−22	2.98E−22
0.08	1.11E−23	7.35E−23	1.00E−22	1.15E−22	1.25E−22	1.31E−22	1.36E−22	1.40E−22
0.10	1.04E−23	1.74E−22	2.44E−22	2.83E−22	3.08E−22	3.25E−22	3.38E−22	3.47E−22
0.15	9.36E−24	6.55E−23	8.96E−23	1.03E−22	1.11E−22	1.17E−22	1.22E−22	1.25E−22
0.20	8.57E−24	3.44E−23	4.55E−23	5.17E−23	5.56E−23	5.84E−23	6.04E−23	6.19E−23
0.30	7.46E−24	1.61E−23	1.97E−23	2.18E−23	2.31E−23	2.40E−23	2.47E−23	2.52E−23
0.40	6.69E−24	1.06E−23	1.23E−23	1.32E−23	1.38E−23	1.42E−23	1.45E−23	1.48E−23
0.50	6.11E−24	8.22E−24	9.13E−24	9.63E−24	9.95E−24	1.02E−23	1.03E−23	1.05E−23
0.60	5.65E−24	6.91E−24	7.45E−24	7.75E−24	7.94E−24	8.07E−24	8.17E−24	8.24E−24
0.80	4.97E−24	5.48E−24	5.71E−24	5.83E−24	5.91E−24	5.96E−24	6.00E−24	6.03E−24
1.00	4.47E−24	4.69E−24	4.79E−24	4.84E−24	4.88E−24	4.90E−24	4.92E−24	4.93E−24
1.50	3.64E−24	3.67E−24	3.69E−24	3.70E−24	3.71E−24	3.71E−24	3.71E−24	3.71E−24
2.00	3.12E−24	3.21E−24	3.24E−24	3.26E−24	3.27E−24	3.28E−24	3.29E−24	3.29E−24
3.00	2.51E−24	2.75E−24	2.85E−24	2.91E−24	2.94E−24	2.97E−24	2.98E−24	3.00E−24
4.00	2.16E−24	2.54E−24	2.70E−24	2.79E−24	2.85E−24	2.89E−24	2.92E−24	2.94E−24
5.00	1.92E−24	2.43E−24	2.64E−24	2.76E−24	2.84E−24	2.89E−24	2.93E−24	2.96E−24
6.00	1.76E−24	2.37E−24	2.63E−24	2.78E−24	2.87E−24	2.93E−24	2.98E−24	3.02E−24
8.00	1.55E−24	2.34E−24	2.67E−24	2.86E−24	2.98E−24	3.06E−24	3.12E−24	3.17E−24
10.00	1.42E−24	2.35E−24	2.75E−24	2.98E−24	3.12E−24	3.22E−24	3.29E−24	3.34E−24
15.00	1.25E−24	2.47E−24	2.99E−24	3.28E−24	3.46E−24	3.59E−24	3.69E−24	3.76E−24
E (keV)	LBBi0	LBBi10	LBBi20	LBBi30	LBBi40	LBBi50	LBBi60	LBBi70
	Effective atomic number (Z_{eff})							
0.015	1.19E+00	4.59E+01	6.51E+01	7.57E+01	8.25E+01	8.72E+01	9.07E+01	9.33E+01
0.02	7.42E−01	4.64E+01	6.60E+01	7.69E+01	8.38E+01	8.86E+01	9.22E+01	9.49E+01
0.03	9.91E−01	4.60E+01	6.54E+01	7.61E+01	8.30E+01	8.77E+01	9.12E+01	9.39E+01
0.04	1.54E+00	4.53E+01	6.41E+01	7.45E+01	8.12E+01	8.58E+01	8.92E+01	9.17E+01
0.05	2.37E+00	4.42E+01	6.22E+01	7.21E+01	7.85E+01	8.29E+01	8.61E+01	8.86E+01
0.06	3.42E+00	4.28E+01	5.97E+01	6.91E+01	7.51E+01	7.93E+01	8.23E+01	8.46E+01
0.08	5.94E+00	3.95E+01	5.39E+01	6.19E+01	6.70E+01	7.05E+01	7.31E+01	7.51E+01
0.10	2.63E+00	4.38E+01	6.15E+01	7.13E+01	7.76E+01	8.19E+01	8.51E+01	8.75E+01
0.15	5.69E+00	3.98E+01	5.44E+01	6.26E+01	6.78E+01	7.14E+01	7.40E+01	7.60E+01
0.20	8.87E+00	3.56E+01	4.71E+01	5.35E+01	5.76E+01	6.04E+01	6.25E+01	6.40E+01
0.30	1.36E+01	2.94E+01	3.61E+01	3.99E+01	4.23E+01	4.39E+01	4.51E+01	4.61E+01
0.40	1.63E+01	2.59E+01	3.00E+01	3.22E+01	3.37E+01	3.47E+01	3.54E+01	3.60E+01
0.50	1.78E+01	2.39E+01	2.66E+01	2.80E+01	2.90E+01	2.96E+01	3.01E+01	3.05E+01
0.60	1.86E+01	2.28E+01	2.46E+01	2.56E+01	2.62E+01	2.66E+01	2.70E+01	2.72E+01
0.80	1.96E+01	2.16E+01	2.25E+01	2.30E+01	2.33E+01	2.35E+01	2.36E+01	2.38E+01

(*continued on next page*)

Table 3 (*continued*)

E (keV)	LBBi0	LBBi10	LBBi20	LBBi30	LBBi40	LBBi50	LBBi60	LBBi70
	Effective atomic number (Z_{eff})							
1.00	2.00E+01	2.10E+01	2.14E+01	2.17E+01	2.18E+01	2.19E+01	2.20E+01	2.21E+01
1.50	2.04E+01	2.06E+01	2.07E+01	2.07E+01	2.07E+01	2.08E+01	2.08E+01	2.08E+01
2.00	2.02E+01	2.07E+01	2.10E+01	2.11E+01	2.12E+01	2.12E+01	2.13E+01	2.13E+01
3.00	1.97E+01	2.15E+01	2.23E+01	2.28E+01	2.30E+01	2.32E+01	2.34E+01	2.35E+01
4.00	1.91E+01	2.24E+01	2.38E+01	2.46E+01	2.51E+01	2.55E+01	2.57E+01	2.59E+01
5.00	1.84E+01	2.32E+01	2.53E+01	2.65E+01	2.72E+01	2.77E+01	2.81E+01	2.83E+01
6.00	1.79E+01	2.40E+01	2.67E+01	2.82E+01	2.91E+01	2.98E+01	3.02E+01	3.06E+01
8.00	1.69E+01	2.54E+01	2.91E+01	3.12E+01	3.25E+01	3.34E+01	3.40E+01	3.45E+01
10.00	1.61E+01	2.66E+01	3.11E+01	3.37E+01	3.53E+01	3.64E+01	3.72E+01	3.78E+01
15.00	1.46E+01	2.87E+01	3.48E+01	3.82E+01	4.04E+01	4.19E+01	4.30E+01	4.38E+01
E (keV)	LBBi0	LBBi10	LBBi20	LBBi30	LBBi40	LBBi50	LBBi60	LBBi70
	Effective electron density (10^{23} electrons/g) (N_{eff})							
0.015	1.65E−01	6.35E+00	9.01E+00	1.05E+01	1.14E+01	1.21E+01	1.26E+01	1.29E+01
0.02	1.03E−01	6.42E+00	9.13E+00	1.06E+01	1.16E+01	1.23E+01	1.28E+01	1.31E+01
0.03	1.37E−01	6.37E+00	9.05E+00	1.05E+01	1.15E+01	1.21E+01	1.26E+01	1.30E+01
0.04	2.14E−01	6.27E+00	8.87E+00	1.03E+01	1.12E+01	1.19E+01	1.23E+01	1.27E+01
0.05	3.28E−01	6.12E+00	8.61E+00	9.99E+00	1.09E+01	1.15E+01	1.19E+01	1.23E+01
0.06	4.73E−01	5.93E+00	8.27E+00	9.57E+00	1.04E+01	1.10E+01	1.14E+01	1.17E+01
0.08	8.22E−01	5.47E+00	7.46E+00	8.57E+00	9.28E+00	9.77E+00	1.01E+01	1.04E+01
0.10	3.64E−01	6.07E+00	8.51E+00	9.88E+00	1.07E+01	1.13E+01	1.18E+01	1.21E+01
0.15	7.88E−01	5.51E+00	7.54E+00	8.67E+00	9.38E+00	9.88E+00	1.02E+01	1.05E+01
0.20	1.23E+00	4.93E+00	6.52E+00	7.41E+00	7.97E+00	8.36E+00	8.65E+00	8.87E+00
0.30	1.89E+00	4.06E+00	5.00E+00	5.52E+00	5.85E+00	6.08E+00	6.25E+00	6.38E+00
0.40	2.26E+00	3.58E+00	4.15E+00	4.46E+00	4.67E+00	4.80E+00	4.91E+00	4.98E+00
0.50	2.46E+00	3.31E+00	3.68E+00	3.88E+00	4.01E+00	4.10E+00	4.17E+00	4.22E+00
0.60	2.58E+00	3.16E+00	3.40E+00	3.54E+00	3.63E+00	3.69E+00	3.73E+00	3.77E+00
0.80	2.71E+00	2.99E+00	3.11E+00	3.18E+00	3.22E+00	3.25E+00	3.27E+00	3.29E+00
1.00	2.77E+00	2.91E+00	2.97E+00	3.00E+00	3.02E+00	3.04E+00	3.05E+00	3.06E+00
1.50	2.82E+00	2.85E+00	2.86E+00	2.87E+00	2.87E+00	2.87E+00	2.88E+00	2.88E+00
2.00	2.80E+00	2.87E+00	2.90E+00	2.92E+00	2.93E+00	2.94E+00	2.94E+00	2.95E+00
3.00	2.72E+00	2.98E+00	3.09E+00	3.15E+00	3.19E+00	3.22E+00	3.24E+00	3.25E+00
4.00	2.64E+00	3.10E+00	3.30E+00	3.41E+00	3.48E+00	3.53E+00	3.56E+00	3.59E+00
5.00	2.55E+00	3.22E+00	3.50E+00	3.66E+00	3.76E+00	3.83E+00	3.89E+00	3.92E+00
6.00	2.48E+00	3.33E+00	3.70E+00	3.90E+00	4.03E+00	4.12E+00	4.19E+00	4.24E+00
8.00	2.34E+00	3.52E+00	4.03E+00	4.32E+00	4.50E+00	4.62E+00	4.71E+00	4.78E+00
10.00	2.22E+00	3.68E+00	4.31E+00	4.66E+00	4.88E+00	5.04E+00	5.15E+00	5.24E+00
15.00	2.02E+00	3.98E+00	4.82E+00	5.29E+00	5.59E+00	5.79E+00	5.95E+00	6.06E+00

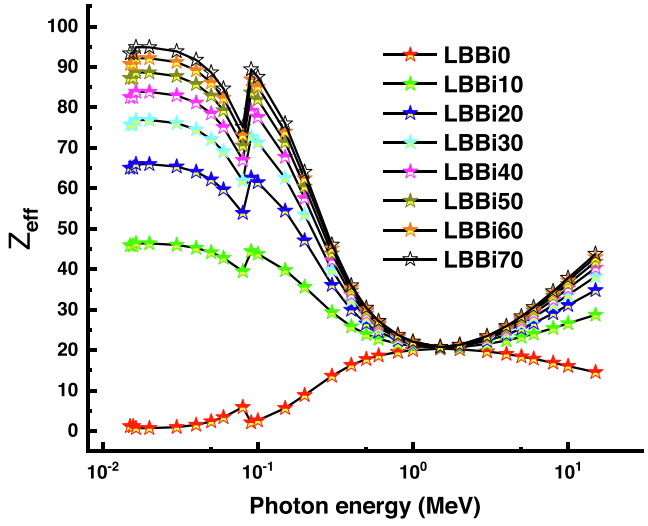

Fig. 10. Variation of effective atomic number (Z_{eff}) with photon energy for all glasses.

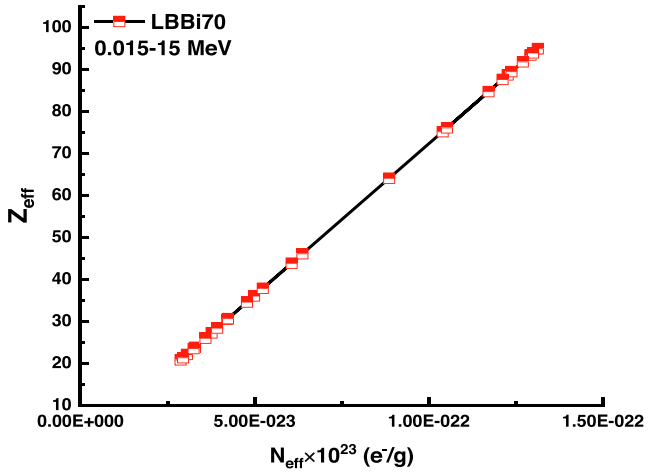

Fig. 11. Variation of effective atomic number (Z_{eff}) with effective electron density (N_{eff}) for LBBi70 glass.

Conclusion

In this work, gamma radiation attenuation features were studied for Bi_2O_3-B_2O_3–Li_2O system by evaluating all relevant LAC, MAC, HVL, MFP, RPE, Z_{eff}, and N_{eff}. By having relatively larger ρ, sample LBBi70 holds the greater MAC among all glasses. Glass LBBi70 has the minimal HVL and MFP. Correlatively higher density glass sample has larger LAC, MAC, Z_{eff}, and RPE & lower HVL and MFP derived for sample LBBi70 in all selected glasses specify its superior gamma ray attenuation capacity. All obtained results imply that glass LBBi70 owns favorable nuclear radiation qualities for its usage at radiology centers and nuclear facilities in place of toxic Pb glass and customary concretes as a safe and

Table 4
Elastic parameters for glass samples.

Bi2O3	No. of bonds	Force constant	bulk modulus	Poission's ratio	Average cross-link density	Shear modulus	Longitudinal modulus	Young's modulus
10	0.6654	367	65.11	0.2462	1.673	39.78	118	99.16
20	0.6373	335.3	66.23	0.2353	2.004	42.57	122.8	105.2
30	0.6321	308.7	68.84	0.2289	2.24	45.56	129.4	112
40	0.6236	285.1	70.74	0.2211	2.572	48.47	135.2	118.4
50	0.6101	264.4	71.61	0.215	2.875	50.38	138.6	122.4
60	0.5976	245.3	72.25	0.2114	3.08	51.64	140.9	125.1
70	0.5834	228.6	72.38	0.2068	3.357	52.74	142.5	127.3

promising shield to minimize the harmful impacts of radiation on the medical staff and radiation workers.

CRediT authorship contribution statement

A. El-Denglawey: Conceptualization, Funding acquisition, Writing - original draft. **Hesham M.H. Zakaly:** Conceptualization, Methodology, Writing - original draft, Investigation. **K. Alshammari:** Writing - original draft, Investigation, Conceptualization. **Shams A.M. Issa:** Conceptualization, Investigation, Methodology, Supervision. **H.O. Tekin:** Investigation, Conceptualization, Supervision. **Yasser B. Saddeek:** Investigation, Conceptualization, Supervision.

Declaration of Competing Interest

The authors declare that they have no known competing financial interests or personal relationships that could have appeared to influence the work reported in this paper.

Acknowledgement

Taif University Researchers Supporting Project number (TURSP-2020/45) Taif University, Taif, Saudi Arabia.

References

[1] Eskalen H, Kavun Y, Kerli S, Eken S. An investigation of radiation shielding properties of boron doped ZnO thin films. Opt Mater 2020;105:109871. https://doi.org/10.1016/j.optmat.2020.109871.
[2] Issa SAM, Mostafa AMA, Hanafy TA, Dong M, Xue X. Comparison study of photon attenuation characteristics of Poly vinyl alcohol (PVA) doped with Pb(NO3)2 by MCNP5 code, XCOM and experimental results. Prog Nucl Energy 2019;111:15–23. https://doi.org/10.1016/j.pnucene.2018.10.018.
[3] Kavaz E, Tekin HO, Kilic G, Susoy G. Newly developed Zinc-Tellurite glass system: An experimental investigation on impact of Ta2O5 on nuclear radiation shielding ability. J Non-Cryst Solids 2020;544:120169. https://doi.org/10.1016/j.jnoncrysol.2020.120169.
[4] Issa SAM, Sayyed MI, Kurudirek M. Study of gamma radiation shielding properties of ZnO-TeO2 glasses. Bull Mater Sci 2017;40:841–57.
[5] Yildiz Yorgun N, Kavaz E, Tekin HO, Sayyed MI, Özdemir F. Borax effect on gamma and neutron shielding features of lithium borate glasses: An experimental and Monte Carlo studies. Mater Res Express 2019;6:115217. https://doi.org/10.1088/2053-1591/ab4fcc.
[6] Ylldlz YN. Gamma-ray shielding parameters of Li2B4O7 glasses: Undoped and doped with magnetite, siderite and Zinc-Borate minerals cases. Radiochim Acta 2019;107:755–65. https://doi.org/10.1515/ract-2019-0014.
[7] Mostafa AMA, Zakaly HMH, Al-Ghamdi SA, Issa SAM, Al-Zaibani M, Ramadan RM, El Agammy EF. PbO–Sb2O3–B2O3–CuO glassy system: Evaluation of optical, gamma and neutron shielding properties. Mater Chem Phys 2021;258:123937. https://doi.org/10.1016/j.matchemphys.2020.123937.
[8] Issa SAM, Hamdalla TA, Darwish AAA. Effect of ErCl 3 in gamma and neutron parameters for different concentration of ErCl 3 -SiO 2 (EDFA) for the signal protection from nuclear radiation. J Alloy Compd 2017;698:234–40.
[9] Elazaka AI, Zakaly HMH, Issa SAM, Rashad M, Tekin HO, Saudi HA, Gillette VH, Erguzel TT, Mostafa AG. New approach to removal of hazardous Bypass Cement Dust (BCD) from the environment: 20Na2O-20BaCl2-(60-x)B2O3-(x)BCD glass system and Optical, mechanical, structural and nuclear radiation shielding competences. J Hazard Mater 2021;403:123738. https://doi.org/10.1016/j.jhazmat.2020.123738.
[10] Abouhaswa AS, Perişanoğlu U, Tekin HO, Kavaz E, Henaish AMA. Nuclear shielding properties of B2O3–Pb3O4–ZnO glasses: Multiple impacts of Er2O3 additive. Ceram Int 2020;46(17):27849–59.
[11] Feller SA, Dell WJ, Bray PJ. 10B NMR studies of lithium borate glasses. J Non-Cryst Solids 1982;51(1):21–30.
[12] Shibata M, Sanchez C, Patel H, Feller S, Stark J, Sumcad G, Kasper J. The density of lithium borate glasses related to atomic arrangements. J Non-Cryst Solids 1986;85(1-2):29–41.
[13] Kodama M, Matsushita T, Kojima S. Velocity of sound and elastic properties of li2O-b2O3 glasses. Jpn J Appl Phys 1995;34:2570–4. https://doi.org/10.1143/JJAP.34.2570.
[14] Simon S, Todea M. Spectroscopic study on iron doped silica-bismuthate glasses and glass ceramics. J Non-Cryst Solids 2006;352(28-29):2947–51.
[15] Baia L, Stefan R, Popp J, Simon S, Kiefer W. Vibrational spectroscopy of highly iron doped B2O3–Bi2O3 glass systems. J Non-Cryst Solids 2003;324(1-2):109–17.
[16] Borsa F, Torgeson DR, Martin SW, Patel HK. Relaxation and fluctuations in glassy fast-ion conductors: Wide-frequency-range NMR and conductivity measurements. Phys. Rev. B 1992;46(2):795–800.
[17] Saddeek YB, Shaaban ER, Moustafa ES, Moustafa HM. Spectroscopic properties, electronic polarizability, and optical basicity of Bi2O3–Li2O–B2O3 glasses. Phys B 2008;403(13-16):2399–407.
[18] Takahashi Y, Yamaguchi K. Dip-coating conditions and modifications of lead titanate and lead zirconate titanate films. J Mater Sci 1990;25(9):3950–5.
[19] Kaewkhao J, Pokaipisit A, Limsuwan P. Study on borate glass system containing with Bi2O3 and BaO for gamma-rays shielding materials: Comparison with PbO. J Nucl Mater 2010;399(1):38–40.
[20] Limkitjaroenporn P, Kaewkhao J, Limsuwan P, Chewpraditkul W. Physical, optical, structural and gamma-ray shielding properties of lead sodium borate glasses. J Phys Chem Solids 2011;72(4):245–51.
[21] Kirdsiri K, Kaewkhao J, Chanthima N, Limsuwan P. Comparative study of silicate glasses containing Bi2O3, PbO and BaO: Radiation shielding and optical properties. Ann Nucl Energy 2011;38(6):1438–41.
[22] Kaewjang S, Maghanemi U, Kothan S, Kim HJ, Limkitjaroenporn P, Kaewkhao J. New gadolinium based glasses for gamma-rays shielding materials. Nucl Eng Des 2014;280:21–6.
[23] Chanthima N, Kaewkhao J, Limkitjaroenporn P, Tuscharoen S, Kothan S, Tungjai M, Kaewjaeng S, Sarachai S, Limsuwan P. Development of BaO–ZnO–B2O3 glasses as a radiation shielding material. Radiat Phys Chem 2017;137:72–7.
[24] Boonin K, Yasaka P, Limkitjaroenporn P, Rajaramakrishna R, Askin A, Sayyed MI, Kothan S, Kaewkhao J. Effect of BaO on lead free zinc barium tellurite glass for radiation shielding materials in nuclear application. J Non-Cryst Solids 2020;550:120386. https://doi.org/10.1016/j.jnoncrysol.2020.120386.
[25] Cheewasukhanont W, Limkitjaroenporn P, Kothan S, Kedkaew C, Kaewkhao J. The effect of particle size on radiation shielding properties for bismuth borosilicate glass. Radiat Phys Chem 2020;172:108791. https://doi.org/10.1016/j.radphyschem.2020.108791.
[26] Kaewjaeng S, Kothan S, Chaiphaksa W, Chanthima N, Rajaramakrishna R, Kim HJ, Kaewkhao J. High transparency La2O3-CaO-B2O3-SiO2 glass for diagnosis x-rays shielding material application. Radiat Phys Chem 2019;160:41–7.
[27] ElBatal FH, Ibrahim S, Abdelghany AM. Optical and FTIR spectra of NdF3-doped borophosphate glasses and effect of gamma irradiation. J Mol Struct 2012;1030:107–12.
[28] ElBatal HA, Abdelghany AM, ElBatal FH, ElBadry KM, Moustaffa FA. UV–visible and infrared absorption spectra of gamma irradiated CuO-doped lithium phosphate, lead phosphate and zinc phosphate glasses: A comparative study. Phys B 2011;406(19):3694–703.
[29] Diab HM, Abdelghany AM, Hafez HS. Dosimetric behavior of modified borate bioglass containing copper for low photon dose measurements using luminescence characteristics. J Mater Sci: Mater Electron 2020;31(22):20452–9.
[30] Issa SAM, Tekin HO. The multiple characterization of gamma, neutron and proton shielding performances of xPbO-(99-x)B2O3–Sm2O3 glass system. Ceram Int 2019;45(17):23561–71.
[31] El-Khayatt AM, Saudy HA. Preparation and characterization of zinc, lanthanum white sand glass for use in nuclear applications. Radiat Phys Chem 2020;166:108497. https://doi.org/10.1016/j.radphyschem.2019.108497.
[32] Bagheri R, Moghaddam AK, Shirmardi SP, Azadbakht B, Salehi M. Determination of gamma-ray shielding properties for silicate glasses containing Bi 2 O 3 , PbO, and BaO. J Non-Cryst Solids 2018;479:62–71.
[33] Kurudirek M, Onaran T. Calculation of effective atomic number and electron density of essential biomolecules for electron, proton, alpha particle and multi-energetic photon interactions. Radiat Phys Chem 2015;112:125–38.
[34] Saudi HA, Abd-Allah WM, Shaaban KS. Investigation of gamma and neutron shielding parameters for borosilicate glasses doped europium oxide for the immobilization of radioactive waste. J Mater Sci: Mater Electron 2020;31(9):6963–76.

[35] Kaçal MR, Akman F, Sayyed MI, Akman F. Evaluation of gamma-ray and neutron attenuation properties of some polymers. Nuclear Engineering and Technology 2019;51(3):818–24.
[36] Tekin HO, Kassab LRP, Kilicoglu O, Magalhães ES, Issa SAM, da Silva Mattos GR. Newly developed tellurium oxide glasses for nuclear shielding applications: An extended investigation. J Non-Cryst Solids 2020;528:119763. https://doi.org/10.1016/j.jnoncrysol.2019.119763.
[37] Heba S, Hassan Y, Tarek E, Borham E, Bendary A. Development of advanced, transparent radiation shielding glass possessing boron and lead ions in the glassy matrix. Egypt J Phys 2020.
[38] Elbashir BO, Dong MG, Sayyed MI, Issa SAM, Matori KA, Zaid MHM. Comparison of Monte Carlo simulation of gamma ray attenuation coefficients of amino acids with XCOM program and experimental data. Results Phys 2018;9:6–11.
[39] Dong MG, El-Mallawany R, Sayyed MI, Tekin HO. Shielding properties of 80TeO2–5TiO2–(15−x) WO3–xAnOm glasses using WinXCom and MCNP5 code. Radiat Phys Chem 2017;141:172–8.
[40] Rashad M, Tekin HO, Zakaly HMH, Pyshkina M, Issa SAM, Susoy G. Physical and nuclear shielding properties of newly synthesized magnesium oxide and zinc oxide nanoparticles. Nuclear Engineering and Technology 2020;52(9):2078–84.
[41] Ferrari a, Sala PR, Fasso A, Ranft J. FLUKA: A Multi-Particle Transport Code. CERN-2005-10 2005:INFN/TC 05/11, SLAC-R-773. https://doi.org/10.2172/877507.
[42] Mostafa AMA, Zakaly HMH, Pyshkina M, Issa SAM, Tekin HO, Sidek HAA, Matori KA, Zaid MHM. Multi-objective optimization strategies for radiation shielding performance of BZBB glasses using Bi2O3: A FLUKA Monte Carlo code calculations. J Mater Res Technol 2020;9(6):12335–45.
[43] Zakaly HM, Abouhaswa AS, Issa SAM, Mostafa MYA, Pyshkina M, El-Mallawany R. Optical and nuclear radiation shielding properties of zinc borate glasses doped with lanthanum oxide. J Non-Cryst Solids 2020;543:120151. https://doi.org/10.1016/j.jnoncrysol.2020.120151.
[44] Henaish AMA, Mostafa M, Salem BI, Zakaly HMH, Issa SAM, Weinstein IA, Hemeda OM. Spectral, electrical, magnetic and radiation shielding studies of Mg-doped Ni–Cu–Zn nanoferrites. J Mater Sci: Mater Electron 2020;31(22):20210–22.
[45] Yasaka P, Pattanaboonmee N, Kim HJ, Limkitjaroenporn P, Kaewkhao J. Gamma radiation shielding and optical properties measurements of zinc bismuth borate glasses. Ann Nucl Energy 2014;68:4–9.
[46] Moustafa ES, Saddeek YB, Shaaban ER. Structural and optical properties of lithium borobismuthate glasses. J Phys Chem Solids 2008;69(9):2281–7.
[47] Bashter II. Calculation of radiation attenuation coefficients for shielding concretes. Ann Nucl Energy 1997;24(17):1389–401.
[48] Issa SAM, Saddeek YB, Tekin HO, Sayyed MI, Shaaban KS. Investigations of radiation shielding using Monte Carlo method and elastic properties of PbO-SiO2-B2O3-Na2O glasses. Curr Appl Phys 2018;18(6):717–27.
[49] Saddeek YB. Study of elastic moduli of lithium borobismuthate glasses using ultrasonic technique. J Non-Cryst Solids 2011;357(15):2920–5.
[50] Doweidar H, Saddeek YB. FTIR and ultrasonic investigations on modified bismuth borate glasses. J Non-Cryst Solids 2009;355(6):348–54.
[51] Saddeek YB, Abousehly AM, Hussien SI. Synthesis and several features of the Na 2 O-B 2 O 3 -Bi 2 O 3 -MoO 3 glasses. J Phys D Appl Phys 2007;40(15):4674–81.
[52] Dutta A, Ghosh A. Ionic conductivity of Li2O–BaO–Bi2O3 glasses. J Non-Cryst Solids 2005;351(3):203–8.
[53] Koshiba K, Honma T, Benino Y, Komatsu T. Patterning and morphology of nonlinear optical GdxBi1-xBO3 crystals in CuO-doped glass by YAG laser irradiation. Appl Phys A 2007;89(4):981–6.
[54] Hall D, Newhouse M, Borrelli N, Lett WD-AP, 1989 U. Nonlinear Measurements of High-Index Glasses n.d.
[55] Saddeek YB, Mohamed HFM, Azooz MA. Structural study of some divalent aluminoborate glasses using ultrasonic and positron annihilation techniques. Phys. Stat. Sol. (a) 2004;201(9):2053–62.
[56] Bridge B, Higazy AA. A model of the compositional dependence of the elastic moduli of polycomponent oxide glasses. Phys Chem Glas 1986;27.
[57] Saddeek YB, Issa SAM, Guclu EEA, Kilicoglu O, Susoy G, Tekin HO. Alkaline phosphate glasses and synergistic impact of germanium oxide (GeO2) additive: Mechanical and nuclear radiation shielding behaviors. Ceram Int 2020;46(10):16781–97.
[58] Saddeek YB. Structural analysis of alkali borate glasses. Phys B 2004;344(1-4):163–75.
[59] Inaba S, Oda S, Morinaga K. Heat capacity of oxide glasses at high temperature region. J Non-Cryst Solids 2003;325(1-3):258–66.